GEOLOGY | THE GEOLOGICAL SOCIETY OF AMERICA®

https://doi.org/10.1130/G50458.1

Manuscript received 28 May 2022
Revised manuscript received 19 July 2022
Manuscript accepted 7 September 2022

Published online 2 December 2022

Diagenetic priming of submarine landslides in ooze-rich substrates

Nan Wu[1], Christopher A.-L. Jackson[2], Michael A. Clare[3], David M. Hodgson[4], Harya D. Nugraha[5], Michael J. Steventon[6] and Guangfa Zhong[1]

[1]State Key Laboratory of Marine Geology, Tongji University, 1239 Siping Road, Shanghai 200092, China
[2]Department of Earth Science and Engineering, Imperial College London, Prince Consort Road, London SW7 2BP, UK
[3]Ocean BioGeosciences, National Oceanography Centre, Southampton SO14 3ZH, UK
[4]School of Earth and Environment, University of Leeds, Leeds LS2 9JT, UK
[5]Center for Sustainable Geoscience, Universitas Pertamina, Jakarta 12220, Indonesia
[6]Shell Research, Shell Centre, London SE1 7NA, UK

ABSTRACT

Oozes are the most widespread deep-sea sediment in the global ocean, but very little is known about how changes in their physical properties during burial impact slope stability and related geohazards. We used three-dimensional seismic reflection, geochemical, and petrophysical data acquired both within and adjacent to 13 large (in total ~6330 km^2) submarine slides on the Exmouth Plateau, North West Shelf, Australia, to investigate how the pre-slide physical properties of oozes control slope failure and emplacement processes. Our integrated data set allows potential slide surfaces to be detected within ooze successions, a crucial advance for improved submarine geohazard assessment. Moreover, we demonstrate that the interplay of tectonics, ocean current activity, and silica diagenesis can prime multiple slides on very low-gradient slopes in tropical oceanic basins. Therefore, the diagenetic state of silica-rich sediments should be considered in future studies to improve slope stability assessments.

INTRODUCTION

Submarine landslides (slides) can trigger tsunami, threaten coastal communities, and damage economically critical seabed infrastructure (e.g., Carter et al., 2012; Clare et al., 2014; Talling et al., 2014). Post-depositional processes can prime substrates to fail, and instantaneous triggers, such as earthquakes, are not prerequisites for slide initiation (Masson et al., 2010; Talling et al., 2014; Urlaub et al., 2018). Such preconditioning appears to be particularly significant for calcareous oozes, because the biogenic constituents that dominate oozes are highly compressible, water rich, and prone to brittle inter-particle cementation, meaning they have distinct geotechnical properties and failure behavior (Tanaka and Locat, 1999; Shiwakoti et al., 2002). During ooze burial, these properties mean calcareous oozes are prone to excess pore pressure buildup, which causes further strength reduction that can ultimately prime the sediment to fail (Tanaka and Locat, 1999). This could explain why large slides occur on unusually low-angle slopes (<2°) in areas of low sediment accumulation (<0.15 m/k.y.) (e.g., Urlaub et al., 2018; Gatter et al., 2021). Despite their apparent significance, the pre-failure physical properties of ooze-rich slopes that ultimately fail remain poorly constrained (Urlaub et al., 2018), because (1) difficulties in directly sampling and geophysically imaging the base of thick (hundreds of meters) slides; and (2) emplacement processes modify the physical properties of the slope sediment.

Identifying potential failure or shear surfaces within sedimentary sequences is crucial for forecasting future events and modeling landslide motion (Locat et al., 2014). Previous studies have focused mostly on individual slides, originating in diatomaceous, rather than calcareous, oozes. Typically, sampling has been from landslide debris; hence, any geotechnically weak layers are unlikely to have been preserved (Locat et al., 2014; Urlaub et al., 2018; Gatter et al., 2021). Therefore, the pre-emplacement physical properties of sediments at basal shear surfaces remain poorly understood, given they can be strongly modified as the slide evolves (Masson et al., 2010). An understanding of the processes and time scales for priming calcareous ooze-rich slides is crucial for improving geohazard assessments, particularly because calcareous oozes constitute >50% of deep ocean floor sediments (Dutkiewicz et al., 2020).

We integrated six time-migrated three-dimensional seismic reflection data sets (over a total of 16,189 km^2; see Appendix S1 in the Supplemental Material[1] for details), a regional network of two-dimensional seismic reflection profiles, and lithological, petrophysical, and geochemical data from Ocean Drilling Program (ODP) Site 762 on the Exmouth Plateau, North West Shelf, Australia (Fig. 1A) to answer the following questions: (1) what are the physical properties of calcareous ooze, and can they explain the stratigraphic occurrence of the basal shear surfaces of large slides?; (2) to what extent does silica diagenesis modify subsurface physical properties and prime substrate for sliding?; and (3) how important are regional tectonic and oceanographic controls in the preconditioning of calcareous-ooze slides?

SETTING AND METHODS

Seismic reflection data from Geoscience Australia (https://www.nopims.gov.au) image 13 submarine slides that cumulatively cover ~6330 km^2 within the upper Miocene to Recent interval of the Exmouth Plateau (horizon H2 to the seabed; Fig. 1B), which is equivalent to

[1]Supplemental Material. Supplemental figures and tables. Please visit https://doi.org/10.1130/GEOL.S.21391233 to access the supplemental material, and contact editing@geosociety.org with any questions.

CITATION: Wu, N., et al., 2023, Diagenetic priming of submarine landslides in ooze-rich substrates: Geology, v. 51, p. 85–90, https://doi.org/10.1130/G50458.1

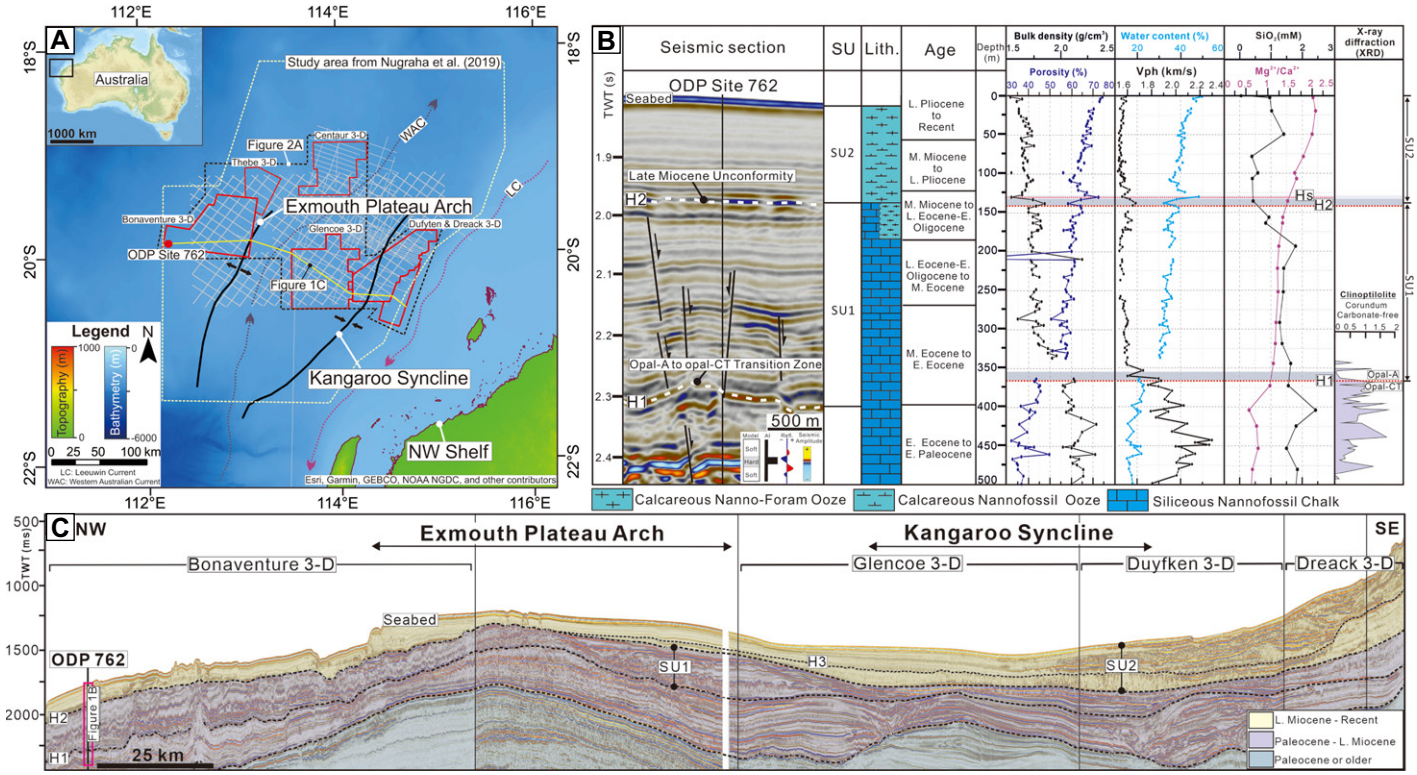

Figure 1. (A) Location of study area on the Exmouth Plateau, Australia. Red polygons and gray lines represent three-dimensional (3-D) and two-dimensional seismic reflection data, respectively. The names of the 3-D seismic data are indicated by labels above the red polygons. (B) Log-seismic integration at Ocean Drilling Program (ODP) Site 762. The legend in the seismic section indicates a downward increase and decrease in acoustic impedance expressed as blue (negative) and red (positive) reflection events, respectively. The horizontal gray bars represent the interval of H1, H2, and Hs observed from the well data. H—seismic horizon; SU—seismic unit; Lith.—lithology; Vph—p-wave velocity. (C) Regional composite seismic section showing main tectonic elements and seismic units. TWT—two-way traveltime; L.—late; M.—middle; E.—early.

seismic unit 3 of Nugraha et al. (2019). Industry and ODP Site 762 boreholes indicate this interval comprises calcareous oozes (Nugraha et al., 2019). ODP Site 762 is unaffected by sliding but intersects an interval stratigraphically equivalent to that hosting the slides; hence, we are able to characterize the pre-failure stratigraphy (Figs. 2A and 2B). We mapped three age-constrained seismic horizons (H1–H3) that define distinct changes in seismic facies and thus bound two seismic units (SU1 and SU2): (1) H1, intra–upper Eocene; (2) H2, the late Miocene unconformity; and (3) H3, an undated horizon that defines the top surface of the largest slide (slide 1; 2800 km^2), which merges with H2 near the Exmouth Plateau Arch (Fig. 1C). Variance attributes (see Appendix S2 for an explanation) were generated to determine the extent and geometry of the depositional bodies. Seismic reflection data were tied to ODP Site 762 (see Appendix S3 for details), allowing us to corelate seismic character and sediment properties. Velocity and density data from ODP Site 762 provide a proxy record of sediment overpressure (Tingay et al., 2009), whereas water content and void ratio were used as proxies for sediment shear strength and compressibility (Tanaka and Locat, 1999; Gatter et al., 2020).

RESULTS

Horizon H1: Opal-A to Opal-CT Conversion Boundary

Horizon H1 defines the base of seismic unit SU1 (Fig. 1C) and is offset by numerous, low-throw (<20 ms two-way traveltime [TWT]) polygonal faults that terminate at or just below horizon H2 (Figs. 1B and 2C). Well-log data reveal a distinct change in petrophysical properties downward with depth across H1, defined by a sharp increase in bulk density (from 1.80 g/cm^3 to 2.17 g/cm^3) and p-wave velocity (from 1.62 km/s to 1.86 km/s) and a decrease in porosity (from 58.0% to 42.5%) and water content (from 30.0% to 20.7%) (Fig. 1B). This dramatic downward change with depth in physical properties is expressed in the seismic reflection data by a discrete package, ~40 ms TWT thick, of high-amplitude reflections, broadly defined at its top by a positive polarity event (i.e., a downward increase in acoustic impedance; Figs. 1B and 2C). X-ray diffraction measurements from ODP Site 762 also show that sediments above H1 have high concentrations of opal-A, whereas below H1, the sediment has high concentrations of opal-CT (Fig. 1B). H1 therefore corresponds to the opal-A to opal-CT conversion boundary (Shipboard Scientific Party, 1990; Nähr et al., 1998).

Seismic Unit SU1: Lower Eocene to upper Miocene Chalk Affected by Silica Diagenesis

The basal part of seismic unit SU1 is enriched in clinoptilolite (Fig. 1B), one of the most common authigenic silicate minerals in pelagic sediments (Nähr et al., 1998). SU1 transitions upward from competent, hard chalk (lower Eocene–upper Eocene) to calcareous ooze (upper Eocene–middle Miocene) (Fig. 1B), and it is deformed by the polygonal fault system offsetting horizon H1 (Fig. 2C). Data from ODP Site 762 show that the dissolved SiO_2 content increases over a 50-m-thick interval near the top of SU1 (Fig. 1B). The dominant diagenetic process associated with SU1 is therefore interpreted to be silica diagenesis, with the locally abundant clinoptilolite interpreted to be caused by the conversion of opal-A to opal-CT (Volpi et al., 2003).

Horizon H2: Late Miocene Unconformity and Regional Failure Plane for Slides

Horizon H2 is a seismically defined reflection that marks the base of seismic unit SU2 (Figs. 2C and 3A; Appendix S4 for slides 2–13). The bases of all 13 slides identified in this unit are on, or only 15–30 m above, H2. Well-log

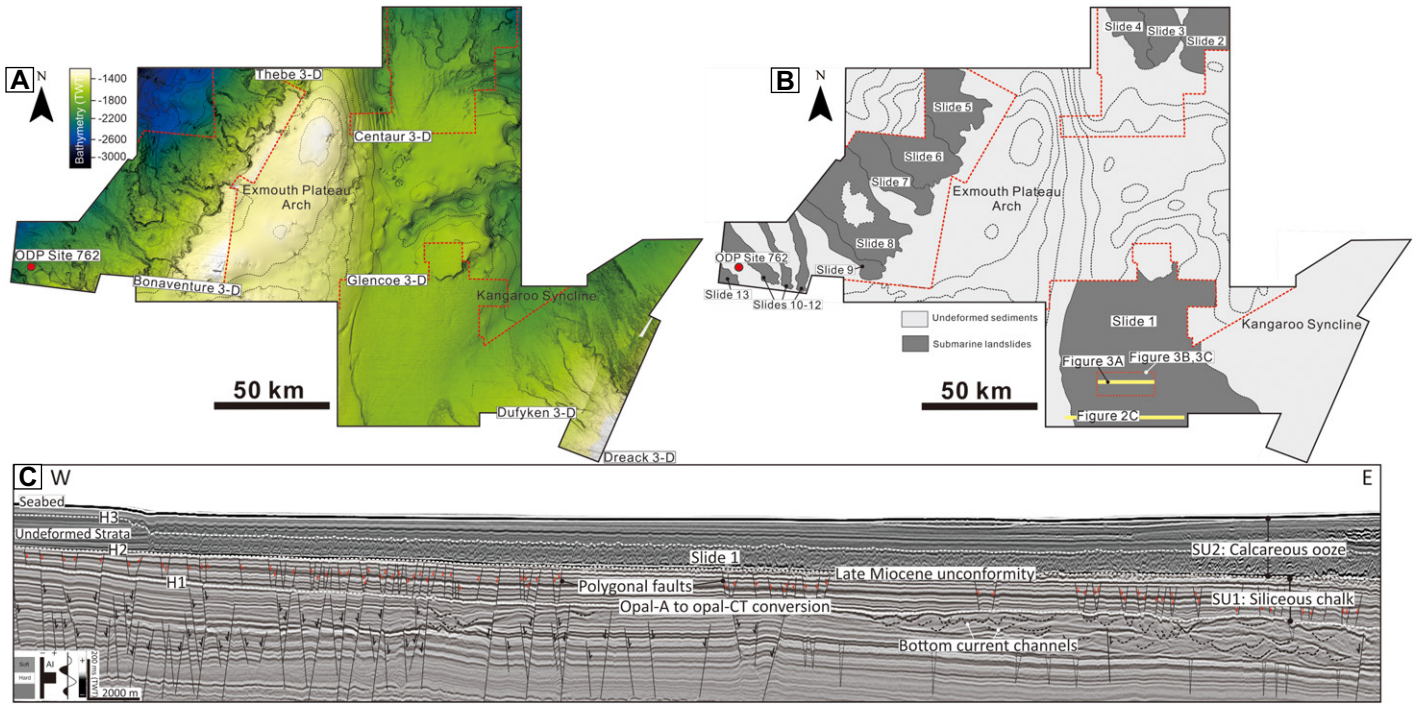

Figure 2. (A) Time structure map (50 m contour interval), showing location of 13 submarine slides that have shaped the seabed of the study area. The labels above the red polygons represent 3-D seismic data names. (B) Sketch of A. (C) Seismic reflection section across slide 1 showing key seismic horizons (H1–H3) and seismic units (SU1 and SU2). The legend in the seismic section indicates a downward increase and decrease in acoustic impedance expressed as black (negative) and white (positive) reflection events, respectively. TWT—two-way traveltime; 3-D—three-dimensional; ODP—Ocean Drilling Program.

data from ODP Site 762 indicate H2 corresponds to a major, biostratigraphically defined unconformity separating upper Eocene and upper Miocene deposits (Shipboard Scientific Party, 1990; Nugraha et al., 2019). H2 defines a sharp upward increase in terrigenous particles (e.g., quartz, feldspar, and clay) and nearshore coccolithophores (e.g., *Braarudosphaera bigelowii*), the latter being extremely unusual for deep-marine basinal sediments and providing possible evidence for an abrupt change in the paleo–ocean current regime associated with Australia-Eurasia

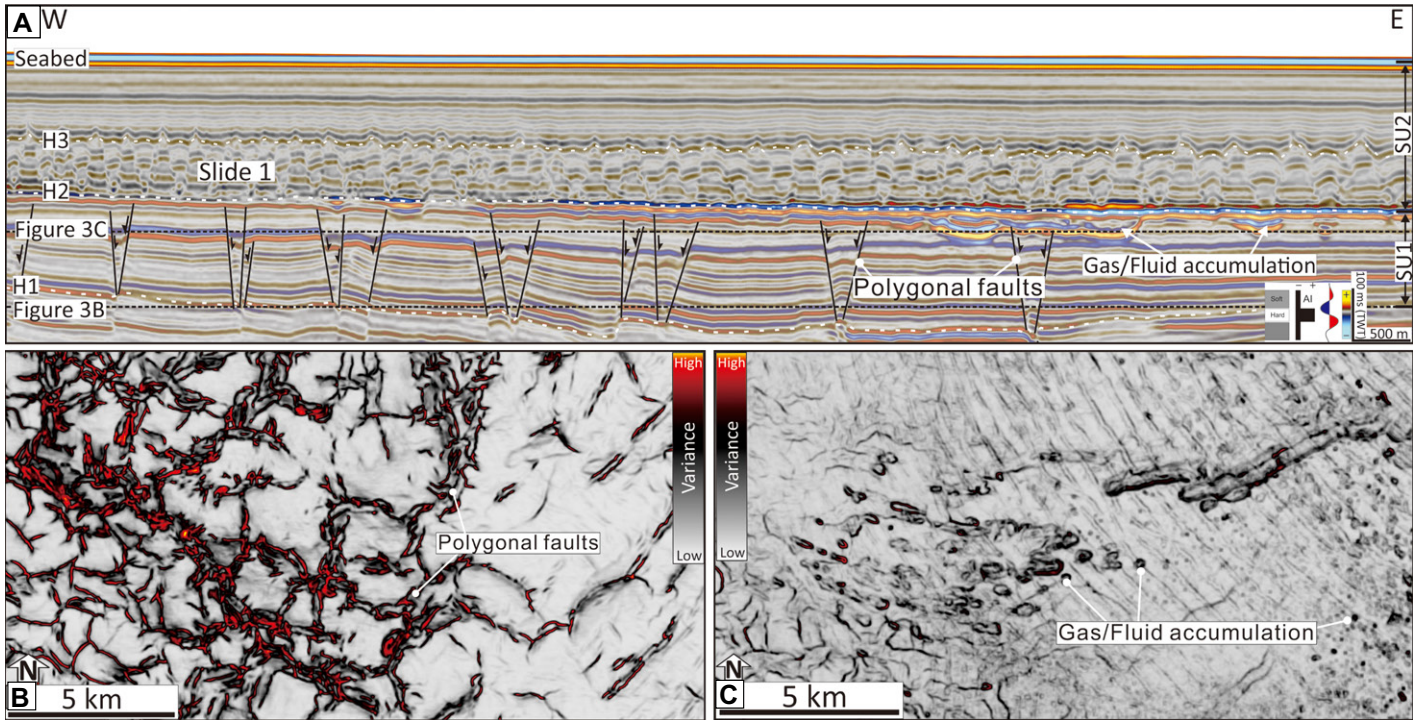

Figure 3. (A) Zoomed-in seismic section of slide 1. H—seismic horizon; SU—seismic unit. (B) Variance time slice calculated at ~130 ms two-way traveltime (TWT) below slide 1, revealing polygonal fault systems. (C) Variance time slice calculated at ~40 ms TWT below slide 1, showing sediment accumulation structures. See Figure 2B for location.

collision during the late Miocene (Shipboard Scientific Party, 1990).

Well-log data reveal horizon H2 defines an ~13-m-thick zone with bulk density increasing downward with depth from 1.60 g/cm^3 to 1.85 g/cm^3 and porosity decreasing downward with depth from 80% to 58.5% (Figs. 1B and 4E). Although we lack direct measurements of permeability, the localized low-porosity and high-density responses within H2 may indicate this unit is overcompacted, with a relatively low permeability compared to the surrounding sediment (Sawyer et al., 2009). Conversely, the localized low-density, low-velocity, and high-porosity responses below H2 may indicate that abnormally high pore pressures have been trapped below this horizon (Fig. 1B; Tingay et al., 2009; Dugan and Sheahan, 2012). It is these sharp changes in petrophysical properties that result in H2 being expressed by a high-amplitude, negative-polarity seismic reflection (Fig. 1B). Another petrophysically distinct interval, Hs (~5 m thick), is revealed only in the well data and is recognized immediately above H2 (Figs. 1B and 4E). Hs is characterized by a decrease in Vp from 1.7 km/s and 1.52 km/s and an increase in water content from 30.0% to 48.5% (Fig. 1B) with decreasing depth. The extremely low-velocity response at the level of Hs indicates possible underpressure at this horizon, whereas the high-water-content response indicates Hs has higher compressibility and lower shear strength relative to the surrounding sediments (Gatter et al., 2020). Nonetheless, direct measurements are needed to achieve a more accurate analysis of the sediment stability than proxy measures from well data, which will improve future hazard assessments (see also Appendix S5).

Seismic Unit SU2: Slide-Prone Calcareous Ooze Interval Affected by Polygonal Faulting and Dewatering

Seismic unit SU2 contains pure calcareous ooze (late Miocene–present) (Fig. 1B) and is dominated by variable-amplitude, discontinuous reflections containing a moderately deformed package of more continuous, moderate- to high-amplitude reflections. The exception to this is near ODP Site 762, where continuous, low-amplitude reflections occur (Fig. 1C). We interpret that the discontinuous and continuous seismic facies represent slide (e.g., Bull et al., 2009) and background slope deposits, respectively.

Slide 1

Slide 1 is the largest and best-imaged slide, and we used it to investigate the role of substrate preconditioning and triggering of slides (Figs. 2A and 2B).

Below slide 1, horizon H1 is crosscut by numerous polygonal faults that tip out upward at or near the basal shear surface of slide 1 (i.e., horizon H2; Figs. 3A and 3B). Horizon H3 defines the top of slide 1 and is a medium-amplitude reflection (Fig. 3A). Directly beneath H2 are numerous high-amplitude, concave reflections that are developed close to the upper termination of the faults (Fig. 3A). In planform, these reflections define subcircular (<100 m in diameter) to elliptical (100–500 m long-axis length) depressions (Fig. 3C), interpreted as localized accumulation of fluid or gas (e.g., Paganoni et al., 2019). The high-amplitude concave reflections resemble zones of fluid expulsion or gas migration as observed elsewhere on the Exmouth Plateau (Paganoni et al., 2019; Foschi and Cartwright, 2020).

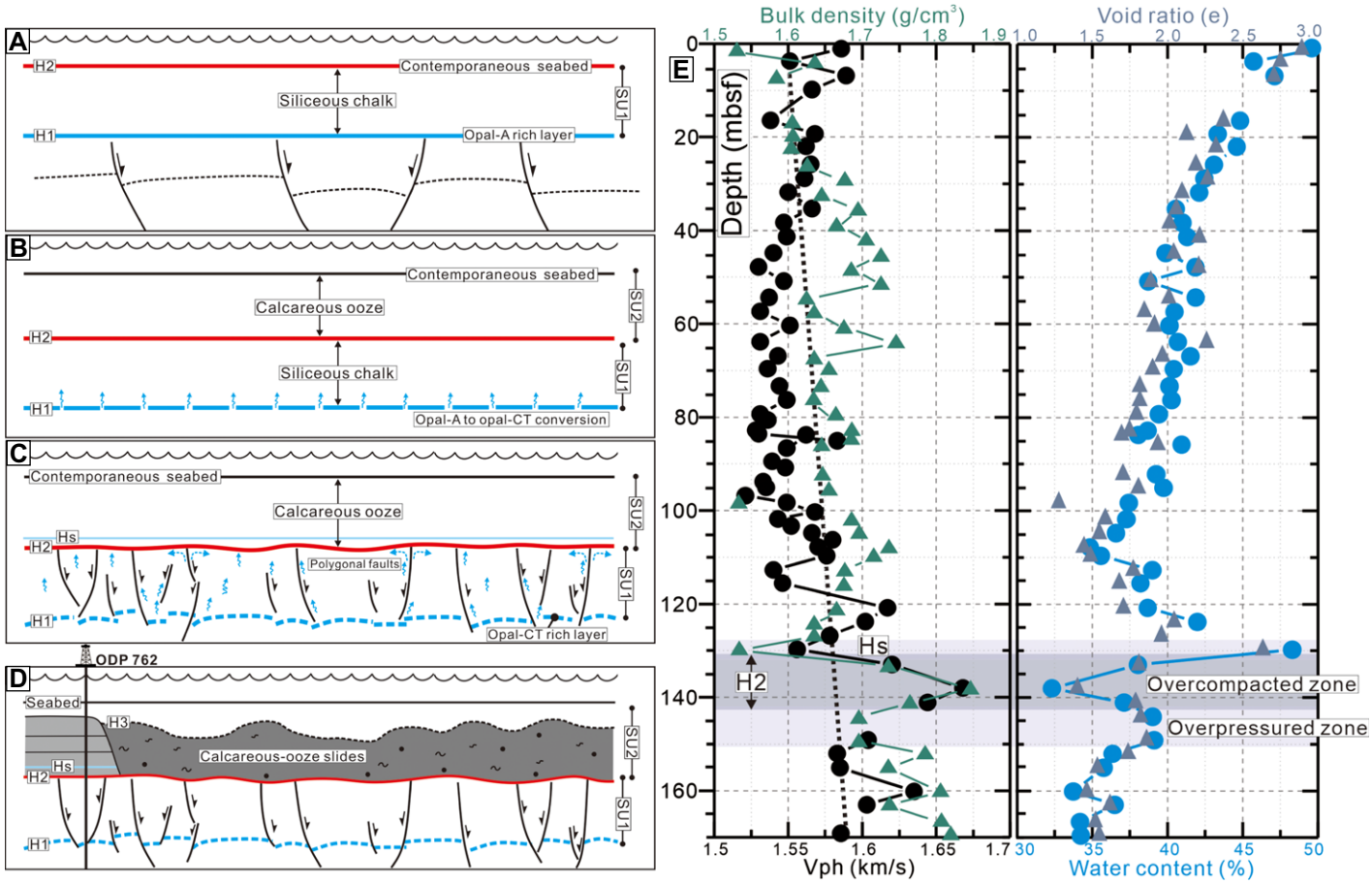

Figure 4. Schematic diagram showing stages of development of submarine slides. (A) Deposition of siliceous chalk. (B) Deposition of calcareous ooze and opal-A–opal-CT conversion. (C) Polygonal faults, fluid migration, and excess pore-pressure generation. (D) Emplacement of regionally distributed slides. (E) Vph, density, water content, and void ratio curves at Ocean Drilling Program Site 762 reveal potential sliding surface (Hs). Vph—p-wave velocity; e—symbol of void ratio; H—seismic horizon; SU—seismic unit; mbsf—meters below seafloor.

DISCUSSION AND CONCLUSION

Controls on the Formation of a Regional Failure Surface and Slide Emplacement

Compared with horizon H2, the 5-m-thick interval Hs is characterized by relatively high water content and void ratio (and hence low shear strength and high compressibility) and a low acoustic velocity, both indicative of overpressure (Fig. 4E). The geotechnical contrast between impermeable strata above H2 and the overlying water-saturated, overpressured ooze of seismic unit SU2 created a weak layer (Hs), providing ideal conditions for slope failure, even on very low-angle slopes. We propose this explanation for why all 13 slides share a stratigraphically equivalent failure surface, with Hs ultimately being locally entrained by the slides.

A similar diagnosis was made in the shallower-water Finneidfjord in Norway, where multiple, asynchronous fjord-flank slides share a regional failure plane, above which a low-density, overpressured layer was deposited (L'Heureux et al., 2012). While the source of the weak layer was terrestrially derived mud and not deep-water calcareous ooze, the similarity of a highly compressible fluid-charged mud overlying an impermeable basal layer is striking. Overpressure in Finneidfjord is related to the infiltration of meteoric groundwater. However, such terrestrially linked charging is not possible in the deep-water setting of the Exmouth Plateau, thus we discuss alternative mechanisms for overpressure development and subsequent slope failure.

Silica Diagenesis as a Primer for Slope Instability and Failure, and Slide Emplacement

We suggest that the most likely source for overpressure relates to the generation and release of fluids during silica diagenesis, which is a well-known dehydration reaction (e.g., Volpi et al., 2003; Davies et al., 2009). In the Exmouth Plateau, silica diagenesis occurred after the calcareous ooze overburden was presented in seismic unit SU2, followed by fluid expulsion and polygonal fault generation (Figs. 4A–4C; Appendix S6). The pronounced decrease in porosity and water content with depth below horizon H1 suggests a large amount of fluid was expelled from the opal-A–opal-CT conversion zone (Fig. 4C; Davies and Clark, 2006). This fluid migrated upward, likely along polygonal faults (e.g., Gay et al., 2006; Davies et al., 2009), and became trapped beneath the lower-permeability horizon H2, forming stratigraphically controlled overpressure and lowering the sediment shear strength (Figs. 4C and 4D). Whether such fluid migration is steady and continuous or is intermittent, perhaps triggered by transient periods of seismicity, is unclear (e.g., Embriaco et al., 2014). The continuous overburden from calcareous oozes could also lead to excess pore pressure and ultimately destabilize a low-gradient slope (Tanaka and Locat, 1999). Moreover, it is plausible that enhanced seismicity, as a result of the Australian and Eurasian plates colliding during the early Miocene, triggered fluid flow and even slope failure (Nugraha et al., 2019). Regardless, our findings support silica diagenesis priming submarine slope instability and the emplacement of a slide ($\sim$110 km^2 in area), which is a mechanistic control proposed for slides in other slope successions (Davies and Clark, 2006; Volpi et al., 2003). Our study is the first to show that silica diagenesis can form a regional failure plane for multiple, large-volume submarine landslides and to identify this control in a tropical setting.

Role of Tectonics and Paleoceanography in Priming and Dictating the Location of Slope Failure

During the late Miocene, the collision of the Australian and Eurasian plates caused the Indonesian ocean gateway to narrow offshore northern Australia (Nugraha et al., 2019). This increased the strength of the southward-flowing Leeuwin Current and suppressed the deep northward-flowing Western Australian Current (Rai and Singh, 2001). These tectonically driven variations fundamentally controlled the benthic and planktonic foraminiferal assemblages (Kennett et al., 1985) and hence the abrupt contrast in lithology and physical properties at horizon H2 that subsequently primed slide failure depth and location. The interplay of multiple physical processes on slide preconditioning can be felt thousands or even millions of years after their activity ceased (Gatter et al., 2020), thus cautioning against the simplistic linkage of sliding to an external trigger. We suggest that such a temporally buffered connection likely exists for many other settings, where diverse tectonic, sedimentological, and/or oceanographic process interactions form stratigraphically constrained fluid sources, pathways, and permeability barriers (Gatter et al., 2020, 2021).

ACKNOWLEDGMENTS

We thank Geoscience Australia for providing the seismic reflection data. We thank the editor, Gerald Dickens, who handled our manuscript, and Morelia Urlaub and two anonymous reviewers for positive feedback that significantly improved the manuscript. We also thank Howard Johnson, Wei Li and Qiliang Sun for helpful discussions while preparing the manuscript.

REFERENCES CITED

Bull, S., Cartwright, J., and Huuse, M., 2009, A review of kinematic indicators from mass-transport complexes using 3D seismic data: Marine and Petroleum Geology, v. 26, p. 1132–1151, https://doi.org/10.1016/j.marpetgeo.2008.09.011.

Carter, L., Milliman, J.D., Talling, P.J., Gavey, R., and Wynn, R.B., 2012, Near-synchronous and delayed initiation of long run-out submarine sediment flows from a record-breaking river flood, offshore Taiwan: Geophysical Research Letters, v. 39, L12603, https://doi.org/10.1029/2012GL051172.

Clare, M.A., Talling, P.J., Challenor, P., Malgesini, G., and Hunt, J., 2014, Distal turbidites reveal a common distribution for large (>0.1 km^3) submarine landslide recurrence: Geology, v. 42, p. 263–266, https://doi.org/10.1130/G35160.1.

Davies, R.J., and Clark, I.R., 2006, Submarine slope failure primed and triggered by silica and its diagenesis: Basin Research, v. 18, p. 339–350, https://doi.org/10.1111/j.1365-2117.2006.00297.x.

Davies, R.J., Ireland, M.T., and Cartwright, J.A., 2009, Differential compaction due to the irregular topology of a diagenetic reaction boundary: A new mechanism for the formation of polygonal faults: Basin Research, v. 21, p. 354–359, https://doi.org/10.1111/j.1365-2117.2008.00389.x.

Dugan, B., and Sheahan, T.C., 2012, Offshore sediment overpressures of passive margins: Mechanisms, measurement, and models: Reviews of Geophysics, v. 50, RG3001, https://doi.org/10.1029/2011RG000379.

Dutkiewicz, A., Judge, A., and Müller, R.D., 2020, Environmental predictors of deep-sea polymetallic nodule occurrence in the global ocean: Geology, v. 48, p. 293–297, https://doi.org/10.1130/G46836.1.

Embriaco, D., et al., 2014, Monitoring of gas and seismic energy release by multiparametric benthic observatory along the North Anatolian Fault in the Sea of Marmara (NW Turkey): Geophysical Journal International, v. 196, p. 850–866, https://doi.org/10.1093/gji/ggt436.

Foschi, M., and Cartwright, J.A., 2020, Seal failure assessment of a major gas field via integration of seal properties and leakage phenomena: American Association of Petroleum Geologists Bulletin, v. 104, p. 1627–1648, https://doi.org/10.1306/02282018111.

Gatter, R., Clare, M.A., Hunt, J.E., Watts, M., Madhusudhan, B.N., Talling, P.J., and Huhn, K., 2020, A multi-disciplinary investigation of the AFEN Slide: The relationship between contourites and submarine landslides, *in* Georgiopoulou, A., et al., eds., Subaqueous Mass Movements and their Consequences: Advances in Process Understanding, Monitoring and Hazard Assessments: Geological Society, London, Special Publication 500, p. 173–193, https://doi.org/10.1144/SP500-2019-184.

Gatter, R., Clare, M.A., Kuhlmann, J., and Huhn, K., 2021, Characterisation of weak layers, physical controls on their global distribution and their role in submarine landslide formation: Earth-Science Reviews, v. 223, 103845, https://doi.org/10.1016/j.earscirev.2021.103845.

Gay, A., Lopez, M., Cochonat, P., Séranne, M., Levaché, D., and Sermondadaz, G., 2006, Isolated seafloor pockmarks linked to BSRs, fluid chimneys, polygonal faults and stacked Oligocene–Miocene turbiditic palaeochannels in the Lower Congo Basin: Marine Geology, v. 226, p. 25–40, https://doi.org/10.1016/j.margeo.2005.09.018.

Kennett, J.P., Keller, G., and Srinivasan, M.S., 1985, Miocene planktonic foraminiferal biogeography and paleoceanographic development of the Indo-Pacific region, *in* Kennett, J. P., ed., The Miocene Ocean: Paleoceanography and Biogeography: Geological Society of America Memoir 163, p. 197–236, https://doi.org/10.1130/MEM163-p197.

L'Heureux, J.-S., et al., 2012, Identification of weak layers and their role for the stability of slopes at Finneidfjord, northern Norway, *in* Yamada, Y., et al., eds., Submarine Mass Movements and Their Consequences: 5th International Symposium, Advances in Natural and Technological

Hazards Research, v. 31, p. 321–330, https://doi.org/10.1007/978-94-007-2162-3_29.
Locat, J., Leroueil, S., Locat, A., and Lee, H., 2014, Weak layers: Their definition and classification from a geotechnical perspective, *in* Krastel, S., et al., eds., Submarine Mass Movements and Their Consequences: 6th International Symposium, Advances in Natural and Technological Hazards Research, v. 37, p. 3–12, https://doi.org/10.1007/978-3-319-00972-8_1.
Masson, D.G., Wynn, R.B., and Talling, P.J., 2010, Large landslides on passive continental margins: Processes, hypotheses and outstanding questions, *in* Mosher, D.C., et al., eds., Submarine Mass Movements and Their Consequences: 4th International Symposium, Advances in Natural and Technological Hazards Research, v. 28, p. 153–165, https://doi.org/10.1007/978-90-481-3071-9_13.
Nähr, T., Botz, R., Bohrmann, G., and Schmidt, M., 1998, Oxygen isotopic composition of low-temperature authigenic clinoptilolite: Earth and Planetary Science Letters, v. 160, p. 369–381, https://doi.org/10.1016/S0012-821X(98)00097-1.
Nugraha, H.D., Jackson, C.A.-L., Johnson, H.D., Hodgson, D.M., and Reeve, M.T., 2019, Tectonic and oceanographic process interactions archived in Late Cretaceous to Present deep-marine stratigraphy on the Exmouth Plateau, offshore NW Australia: Basin Research, v. 31, p. 405–430, https://doi.org/10.1111/bre.12328.
Paganoni, M., King, J.J., Foschi, M., Mellor-Jones, K., and Cartwright, J.A., 2019, A natural gas hydrate system on the Exmouth Plateau (NW shelf of Australia) sourced by thermogenic hydrocarbon leakage: Marine and Petroleum Geology, v. 99, p. 370–392, https://doi.org/10.1016/j.marpetgeo.2018.10.029.
Rai, A.K., and Singh, V.B., 2001, Late Neogene deep-sea benthic foraminifera at ODP Site 762B, eastern Indian Ocean: Diversity trends and palaeoceanography: Palaeogeography, Palaeoclimatology, Palaeoecology, v. 173, p. 1–8, https://doi.org/10.1016/S0031-0182(01)00299-1.
Sawyer, D.E., Flemings, P.B., Dugan, B., and Germaine, J.T., 2009, Retrogressive failures recorded in mass transport deposits in the Ursa Basin, Northern Gulf of Mexico: Journal of Geophysical Research, v. 114, B10102, https://doi.org/10.1029/2008JB006159.
Shipboard Scientific Party, 1990, Introduction, *in* Haq, B.U., von Rad, U., et al., Proceedings of the Ocean Drilling Program, Initial Reports, Volume 122: College Station, Texas, Ocean Drilling Program, p. 9–15, https://doi.org/10.2973/odp.proc.ir.122.103.1990.
Shiwakoti, D.R., Tanaka, H., Tanaka, M., and Locat, J., 2002, Influences of diatom microfossils on engineering properties of soils: Soil and Foundation, v. 42, no. 3, p. 1–17, https://doi.org/10.3208/sandf.42.3_1.
Talling, P.J., Clare, M.L., Urlaub, M., Pope, E., Hunt, J.E., and Watt, S.F.L., 2014, Large submarine landslides on continental slopes: Geohazards, methane release, and climate change: Oceanography (Washington, D.C.), v. 27, p. 32–45, https://doi.org/10.5670/oceanog.2014.38.
Tanaka, H., and Locat, J., 1999, A microstructural investigation of Osaka Bay clay: The impact of microfossils on its mechanical behaviour: Canadian Geotechnical Journal, v. 36, p. 493–508, https://doi.org/10.1139/t99-009.
Tingay, M.R.P., Hillis, R.R., Swarbrick, R.E., Morley, C.K., and Damit, A.R., 2009, Origin of overpressure and pore-pressure prediction in the Baram province, Brunei: American Association of Petroleum Geologists Bulletin, v. 93, p. 51–74, https://doi.org/10.1306/08080808016.
Urlaub, M., Geersen, J., Krastel, S., and Schwenk, T., 2018, Diatom ooze: Crucial for the generation of submarine mega-slides?: Geology, v. 46, p. 331–334, https://doi.org/10.1130/G39892.1.
Volpi, V., Camerlenghi, A., Hillenbrand, C.-D., Rebesco, M., and Ivaldi, R., 2003, Effects of biogenic silica on sediment compaction and slope stability on the Pacific margin of the Antarctic Peninsula: Basin Research, v. 15, p. 339–363, https://doi.org/10.1046/j.1365-2117.2003.00210.x.

Printed in USA